Ferromagnetic Interactions in the First Bis(μ-end-on-azido)manganese(II) Dinuclear Compound: $[Mn(terpy)(N_3)_2]_2 \cdot 2H_2O$

Roberto Cortés,† J. Luis Pizarro,‡ Luis Lezama,† M. Isabel Arriortua,‡ and Teófilo Rojo*,†

Departamentos de Química Inorgánica y Mineralogía-Petrología, Universidad del País Vasco, Aptdo. 644, 48080 Bilbao, Spain

Received November 15, 1993

Introduction

In the recent years, our work in the field of coordination chemistry has been focused on obtaining polynuclear systems showing ferromagnetic type interactions between the metallic centers. Pseudohalide ions are able to bridge the metals in several forms, including *end-to-end* or *end-on* modes. The first type of bridging is known to transmit antiferromagnetic interactions between the metallic centers. However, both the azide and cyanate anions in their *end-on* coordination mode have been shown to be able to transmit ferromagnetic type interactions.[1,2] The first azide[3] and cyanate[4] nickel(II) dinuclear compounds having this kind of bridging have been obtained and characterized. Furthermore, a synthetic strategy has been used to obtain this type of compound showing ferromagnetic exchange coupling.[5]

In the Cu(II) end-on-azido systems, the ferromagnetic interaction has extensively been studied, from a theoretical point of view, by Kahn and co-workers, who have developed the concept of spin polarization induced by the in-plane π_g orbital of the azide anion.[6] The bridging angle has experimentally shown to be the main factor in determining the strength of the ferromagnetic interactions in Ni(II) systems.[3,7] No theoretical study has been carried out concerning ferromagnetically coupled end-on-azido dinuclear complexes with other transition metals. The aim of this paper is to extend the study to other metals in order to determine their influence on both the sign and strength of the exchange coupling. As a result, the first dinuclear Mn(II) system with this kind of bridging has been synthesized.

In this paper we present the crystal structure and the spectroscopic and magnetic properties of bis(μ-end-on-azido)-bis(2,2′:6′,2″-terpyridine)dimanganese(II) dihydrate, $[Mn(terpy)(N_3)_2]_2 \cdot 2H_2O$. The exchange interactions between the manganese cations through the bis(μ-azido) bridges are also analyzed.

Experimental Section

Synthesis. $[Mn(terpy)(N_3)_2] \cdot H_2O$ was prepared by adding an aqueous solution containing 0.395 g (10^{-3} mol) of $Mn(terpy)(Cl)_2 \cdot 2H_2O$ (previously prepared by mixing stoichiometric amounts of manganese(II) chloride and terpy ligand in a methanol/water solution) to a saturated aqueous solution of sodium azide. The resulting precipitate was washed with water and recrystallized in a water/methanol mixture to give yellow-orange crystals adequate for the crystallographic study. The elemental analysis and atomic absorption results were consistent with the formula $C_{15}H_{13}N_9OMn$.

Crystal Structure Determination. A rhombohedral-shaped crystal of approximate dimensions 0.25 × 0.22 × 0.32 mm was sealed in a capillary and used for data collection on an Enraf-Nonius CAD-4 diffractometer. Cell constants and the orientation matrix for data collection were obtained by least-squares refinement of the diffraction data from 25 reflections in the θ range 8–13°. The experimental density was determined by a flotation method in a bromoform/chloroform mixture. Data were collected at 298 K using graphite crystal-monochromatized Mo Kα radiation (λ = 0.710 69 Å). The intensities were corrected for Lorentz and polarization effects and for absorption by an empirical method (DIFABS[8]). The structure was solved via the heavy-atom procedures of Patterson (SHELXS 86[9]) and refined by Fourier syntheses [blocked-matrix least-squares methods (SHELX 76[10])] with scattering factors from ref 11. All non-hydrogen atoms were refined with anisotropic displacement factors. Hydrogen atoms, except those corresponding to the water molecule, were identified in the difference Fourier maps and included in the refinement with isotropic U values. The hydrogens of the water molecule were not located. Final refinement of the obtained model led to convergence at $R = 0.040$ and $R_w = 0.043$. Crystallographic data and processing parameters are given in Table 1, and the final positional parameters are shown in Table 2.

Table 1. Crystallographic Data for $[Mn(terpy)(N_3)_2] \cdot H_2O$

chem formula	$C_{15}H_{13}N_9OMn$	fw	390.27
a	8.575(2) Å	space group (No.)	$P\bar{1}$ (2)
b	10.737(1) Å	T	25 °C
c	10.772(1) Å	ρ_{obsd}	1.54(3) g cm^{-3}
α	70.64(1)°	ρ_{calcd}	1.55 g cm^{-3}
β	69.10(1)°	μ	7.81 cm^{-1}
γ	68.20(1)°	λ	0.710 69 Å
V	837.3(2) Å^3	$R(F_o)^a$	0.040
Z	2	$R_w(F_o)^b$	0.043

^{a} $R(F_o) = [\sum||\Delta F|/\sum|F_o|]$. ^{b} $R_w(F_o) = [\sum w(|\Delta F|)^2/\sum w|F_o|^2]^{1/2}$. The final $\rho_{max}^+/\rho_{max}^-$ values (e/Å^{-3}) were +0.337/−0.279.

Table 2. Atomic Coordinates and Equivalent Isotropic Temperature Factors (Å^2) for the Non-Hydrogen Atoms of $[Mn(terpy)(N_3)_2] \cdot H_2O$

atom	x	y	z	B_{eq}^a
Mn	0.14054(6)	0.33726(5)	0.47369(4)	4.86(1)
N1	0.3874(3)	0.3911(3)	0.3310(2)	5.35(8)
N2	0.2167(3)	0.2597(2)	0.2857(3)	5.06(7)
N3	−0.0565(3)	0.2324(2)	0.4946(3)	5.51(8)
N4	0.0178(4)	0.4577(3)	0.6295(2)	5.68(8)
N5	0.0066(4)	0.4233(3)	0.7481(3)	5.68(9)
N6	−0.0009(5)	0.3938(4)	0.8616(3)	9.40(14)
N7	0.2793(4)	0.1707(4)	0.6032(4)	7.51(12)
N8	0.2697(4)	0.1020(3)	0.7072(3)	7.25(12)
N9	0.2669(9)	0.0269(5)	0.8119(5)	16.08(31)
Ow	0.1593(6)	0.8669(4)	0.0781(4)	12.95(16)
C1	0.4691(5)	0.4594(4)	0.3589(4)	6.68(12)
C2	0.6199(5)	0.4880(4)	0.2749(4)	6.93(12)
C3	0.6947(5)	0.4427(4)	0.1571(4)	6.57(12)
C4	0.6145(5)	0.3714(4)	0.1253(3)	6.07(11)
C5	0.4595(4)	0.3483(3)	0.2136(3)	4.94(9)
C6	0.3591(4)	0.2779(3)	0.1864(3)	5.24(10)
C7	0.4043(5)	0.2365(4)	0.0660(4)	7.24(13)
C8	0.2978(6)	0.1780(4)	0.0497(4)	9.08(16)
C9	0.1491(6)	0.1609(4)	0.1507(4)	8.15(14)
C10	0.1124(4)	0.2023(3)	0.2697(3)	5.83(9)
C11	−0.0393(4)	0.1852(3)	0.3882(4)	5.79(10)
C12	−0.1565(5)	0.1220(4)	0.3916(5)	7.31(13)
C13	−0.2920(5)	0.1083(4)	0.5055(5)	8.84(17)
C14	−0.3091(5)	0.1545(4)	0.6137(5)	7.28(13)
C15	−0.1880(5)	0.2165(4)	0.6058(4)	6.78(13)

^{a} $B_{eq} = (8\pi^2/3)\sum_i\sum_j U_{ij} a_i^* a_j^* \mathbf{a}_i \cdot \mathbf{a}_j$.

† Departamento de Química Inorgánica.
‡ Departamento de Mineralogía-Petrología.

(1) Commarmond, J.; Plumere, P.; Lehn, J. M.; Agnus, Y.; Louis, R.; Weiss, R.; Kahn, O.; Morgenstern-Badarau, I. *J. Am. Chem. Soc.* **1982**, *104*, 6330.
(2) Sikorav, R. E.; Bkouche-Waksman, I.; Kahn, O. *Inorg. Chem.* **1984**, *23*, 490.
(3) Arriortua, M. I.; Cortés, R.; Lezama, L.; Rojo, T.; Soláns, X.; Font-Bardia, M. *Inorg. Chim. Acta* **1990**, *174*, 263.
(4) Arriortua, M. I.; Cortés, R.; Mesa, J. L.; Lezama, L.; Rojo, T.; Villeneuve, G. *Transition Met. Chem.* **1988**, *13*, 371.
(5) Rojo, T.; Lezama, L.; Cortés, R.; Mesa, J. L.; Arriortua, M. I.; Villeneuve, G. *J. Magn. Magn. Mater.* **1990**, *83*, 519.
(6) Charlot, M. F.; Kahn, O.; Chaillet, M.; Larrieu, C. *J. Am. Chem. Soc.* **1986**, *108*, 2574 and references therein.
(7) Cortés, R.; Ruiz de Larramendi, J. I.; Lezama, L.; Rojo, T.; Urtiaga, M. K.; Arriortua, M. I. *J. Chem. Soc., Dalton Trans.* **1992**, 2723.
(8) Walker, N.; Stuart, D. *Acta Crystallogr.* **1983**, *A39*, 158.
(9) Sheldrick, G. M. SHELXS86. *Acta Crystallogr.* **1990**, *A46*, 467.
(10) Sheldrick, G. M. SHELX-76: A Program for Crystal Structure Determination. University Chemical Laboratory, Cambridge, U.K., 1976.
(11) *International Tables for X-Ray Crystallography*; Kynoch Press: Birmingham, U.K., 1974; Vol. IV, pp 99, 149.

0020-1669/94/1333-2697$04.50/0 © 1994 American Chemical Society

Table 3. Selected Bond Distances (Å) and Angles (deg) for $[Mn(terpy)(N_3)_2]\cdot H_2O$[a]

	Manganese Coordination Sphere		
Mn–N1	2.275(3)	Mn–N2	2.233(3)
Mn–N3	2.268(3)	Mn–N4	2.182(3)
Mn–N4^i	2.272(2)	Mn–N7	2.123(3)
Mn···Mn^i	3.5250(6)	Mn···Mn^{ii}	7.5754(6)
N1–Mn–N2	71.08(9)	N1–Mn–N3	142.8(1)
N1–Mn–N4	110.8(1)	N1–Mn–N7	92.7(1)
N1–Mn–N4^i	88.7(1)	N2–Mn–N3	71.7(1)
N2–Mn–N4	164.7(1)	N2–Mn–N7	103.2(1)
N2–Mn–N4^i	89.61(9)	N3–Mn–N4	105.2(1)
N3–Mn–N7	95.5(1)	N3–Mn–N4^i	91.2(1)
N4–Mn–N7	92.0(1)	N4–Mn–N4^i	75.4(1)
N7–Mn–N4^i	166.9(1)	Mn–N4–Mn^i	104.6(1)
	Azide Groups		
N4–N5	1.185(4)	N5–N6	1.141(5)
N7–N8	1.113(5)	N8–N9	1.146(5)
Mn–N4–N5	130.3(2)	Mn–N7–N8	145.3(4)
N4–N5–N6	177.4(4)	N7–N8–N9	176.8(5)

[a] i = $-x$, $1-y$, $1-z$; ii = $1-x$, $-y$, $1-z$.

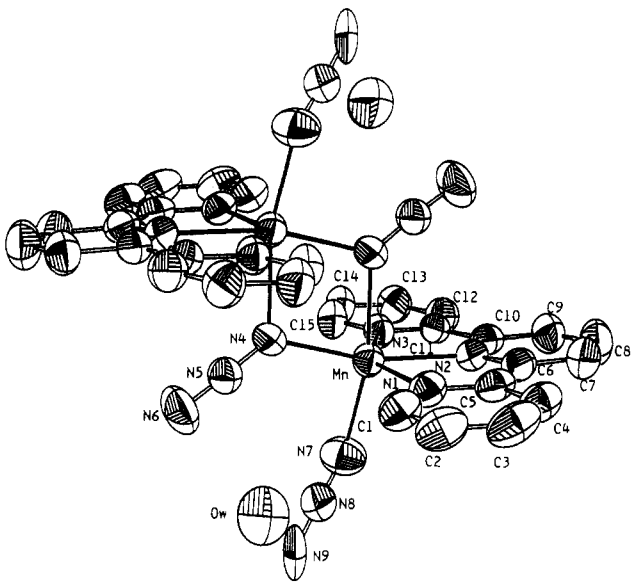

Figure 1. ORTEP view of the $[Mn(terpy)(N_3)_2]_2\cdot 2H_2O$ dimeric compound, showing the atom numbering.

Physical Measurements. Fourier transform infrared spectroscopy on KBr pellets was performed on a Perkin-Elmer 1720X FT-IR instrument, in the 4000–400-cm^{-1} region. Magnetic susceptibilities of powdered samples were carried out in the temperature range 4.2–200 K using a pendulum type susceptometer/magnetometer (Manics DSM8), equipped with a helium continuous-flow cryostat. The experimental susceptibilities were corrected for the diamagnetism of the constituent atoms (Pascal Tables). ESR spectra were recorded, on powdered samples at X-band frequency, with a Bruker ESP 300 spectrometer, equipped with a standard Oxford low-temperature device, calibrated by the NMR probe for the magnetic field, the frequency being measured by a Hewlett Packard 5352B microwave frequency counter.

Results and Discussion

Crystal Structure. Selected bond distances and angles for the compound are compiled in Table 3, and an ORTEP[12] drawing of the dimeric $[Mn(terpy)(N_3)_2]_2\cdot 2H_2O$ complex is shown in Figure 1.

The structure consists of centrosymmetric $[Mn(terpy)(N_3)_2]_2\cdot 2H_2O$ dimers formed by the union of two $Mn(terpy)(N_3)_2\cdot H_2O$ fragments. The manganese(II) ions in the dimer are linked by two end-on bridging azide groups. The other two azides act as terminal ligands (Figure 1). Each manganese cation exhibits a distorted-octahedral coordination sphere, with the three nitrogen atoms of the terpy ligand [Mn–N1,N2,N3: 2.275(3), 2.233(3), 2.268(3) Å] and the nitrogen atom of one bridging azide group [Mn–N4: 2.182(3) Å] forming the equatorial plane. The nitrogen atom of one terminal azido group [Mn–N7: 2.123(3) Å] and the nitrogen atom of the second bridging group [Mn–N4^i: 2.272(2) Å (i = $-x$, $1-y$, $1-z$)] are situated in the axial positions. The manganese(II) ion deviates –0.1958 Å from the average equatorial plane. Distortion of the coordination polyhedron around the Mn(II) from octahedral to trigonal prismatic has been calculated by the Muetterties and Guggenberger model.[13] The resulting value, $\Delta = 0.17$ (supplementary material), indicates that the coordination polyhedron is close to an octahedron. The terpy ligand can be considered as practically planar, with maximum deviations of –0.1051 Å for C4 and +0.0971 Å for C9.

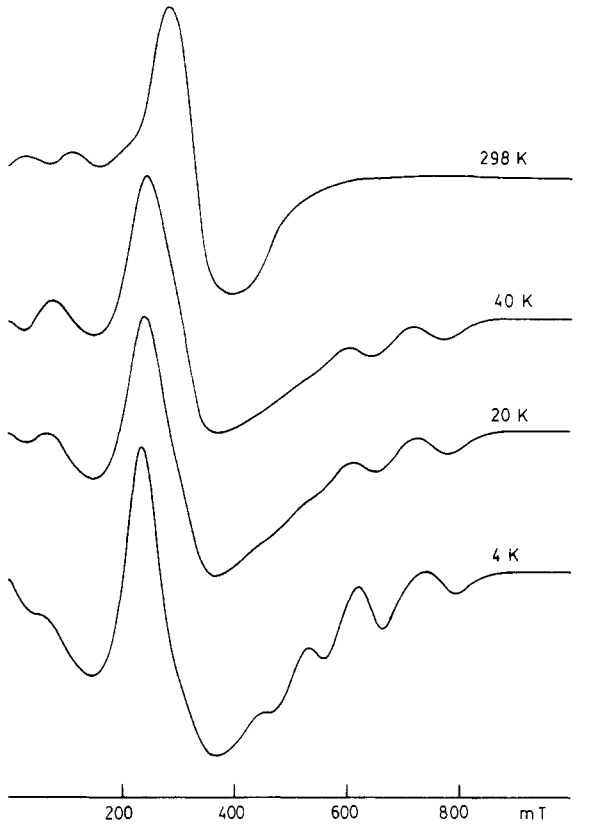

Figure 2. Variation of the X-band ESR spectrum of the title compound with temperature.

The existence of an inversion center causes the Mn–N4–Mn^i–N4^i bridging unit to form a plane. In this dimeric unit, the manganese cations are separated from each other by 3.5250(6) Å. The bridging azides slightly deviate (up and down) from that plane, with a bridging Mn–N4–Mn^i angle of 104.6(1)°. The larger internal distance of the bridging azide (N4–N5 = 1.185) with respect to the terminal one (N7–N8 = 1.113) seems to be related to the bridging situation. The high thermal parameters of the extreme noncoordinating nitrogens of both the bridging and terminal azides do not allow a subtle comparison of the external distances of these groups. The bridging and terminal azido ligands are quasilinear with N4–N5–N6 = 177.4(4)° and N7–N8–N9 = 176.8(5)°, respectively.

Infrared Spectroscopy. The IR spectrum shows a strong broad band with two peaks at 3580 and 3450 cm^{-1}, due to the water molecule.

The $\nu_{asym}(N_3)$ mode appears as a very strong splitting band at 2075 and 2045 cm^{-1}, which is consistent with a structure containing

(12) Johnson, C. K. ORTEP. Report ORNL-3794; Oak Ridge National Laboratory: Oak Ridge, TN, 1965.

(13) Muetterties, E. L.; Guggenberger, G. *J. Am. Chem. Soc.* **1974**, *96*, 1748.

Table 4. Examples of Manganese(II) Dimers with Edge-Sharing Octahedral Topologies[a]

compd	bridge	Mn–Mn, Å	Mn–X, Å	Mn–X′, Å	Δd, Å	Mn–X–Mn, deg	J, cm^{-1}	ref
$[Mn_2(salmp)_2]\cdot 4MeCN$	$(\mu\text{-}O)_2$	3.205	2.183	2.214	0.031	93.6		16
$[Mn_2Cl_2(H_2O)_8](C_{12}H_{24}O_6)$	$(\mu\text{-}Cl)_2$	3.707	2.522	2.535	0.013	94.3		17
$[Mn_2Cl_6(H_2O)_4](CH_3)_2CHNH_3$	$(\mu\text{-}Cl)_2$	3.828	2.570	2.639	0.069	94.6	AF[b]	18
$[Mn_2(sal)_4(MeOH)_2]\cdot MeOH$	$(\mu\text{-}O)_2$	3.305	2.146	2.179	0.033	99.6		16
$[Mn(bpeap)(THF)_2]_2(ClO_4)_2$	$(\mu\text{-}O)_2$	3.256	2.096	2.156	0.060	99.9	–0.36	19
$[Mn(SALPS)]_2$	$(\mu\text{-}O)_2$	3.300	2.129	2.139	0.010	101.2	–1.88	20
$[Mn_2(DBcat)_2(py)_6]$	$(\mu\text{-}O)_2$	3.346	2.096	2.172	0.076	103.2		21
$[Mn_2H_2L1(CH_3COO)]\cdot 2CH_3OH$	$(\mu\text{-}O)_2$	3.340	2.108	2.149	0.041	103.6	F[b]	22
$[Mn(L3)(L4)]_2(ClO_4)_4\cdot 2EtOH$	$(\mu\text{-}O)_2$	3.409	2.150	2.151	0.001	104.9		23
$[Mn(F_6acac)_2AmPh]_2$	$(\mu\text{-}O)_2$	3.465	2.161	2.186	0.025	105.7	–1.99	24
$[Mn(hfac)_2(IMHPH)]_2(NITPH)$	$(\mu\text{-}O)_2$	3.475	2.151	2.165	0.014	107.2	–1.75	25
$[Mn(hfac)_2(IMHPH)(IMPH)]_2$	$(\mu\text{-}O)_2$	3.455	2.159	2.159	0.000	107.3	–2.88	25
$[Mn(terpy)(N_3)_2]_2\cdot 2H_2O$	$(\mu\text{-}N)_2$	3.525	2.182	2.272	0.090	104.6	+2.43	this work

[a] Abbreviations: Δd = (Mn–X′) – (Mn–X); AF = antiferromagnetic; F = ferromagnetic; salmp = 2-(bis(salicylideneamino)methyl)phenolate; $C_{12}H_{24}O_6$ = 18-crown-6; sal = salicylaldehyde; bpeap = *o*-(bis(2-(1-pyrazolyl)ethyl)amino)phenolato; SALPS = *N*,*N*′-[1,1′-dithiobis(phenylene)]bis(salicylideneaminato); DBcat = 3,5-di-*tert*-butylcatechol; L3 = *N*-((2-hydroxyethyl)methyl)-2-pyridylketimine; L4 = (*Z*)-1,3-bis(2-pyridyl)but-2-enone; F_6acac = hexafluoroacetylacetonato; hfac = hexafluoroacetylacetonate; IMHPH = 1-hydroxy-2-phenyl-4,4,5,5-tetramethyl-4,5-dihydroxo-1*H*-imidazole; terpy = 2,2′:6′,2″-terpyridine. [b] The authors believe the compound to have this magnetic behavior.

both end-on bridging and terminal azide ligands. A similar situation is found in the related nickel–azido compounds.[3,7] The azide symmetric stretch, $\nu_{sym}(N_3)$, is observed at about 1300 cm^{-1}, partially obscured by a band of the terpy ligand. The presence of this azide band is in accordance with the existence of end-on bridging or terminal azides (it does not appear for the symmetrical end-to-end azido groups). Finally, the bands appearing at 615 and 605 cm^{-1} correspond to the deformation mode of the azido groups.

ESR and Magnetic Measurements. The variation of the X-band ESR spectra of the title compound with temperature is shown in Figure 2. Several transitions with a certain overlapping appear at room temperature in the 0–100-mT range (see Figure 2). The transitions appear at 50, 137.5, and 332.5 mT. When the sample is cooled a variation of these ESR signals can be observed, which is indicative of a change in the population of the energetic states in the dimer. New signals appearing at lower temperatures are seen at 105, 462.5, 542.5, 645, and 767.5 mT. The two $S = {}^5/_2$ ions from the Mn(II) dimer couple in an exchange interaction to give dimer states with total spins of S = 5, 4, 3, 2, 1, 0. Each state, except the S = 0 one, has a degeneracy ($2S$ + 1) greater than 1 and may have a zero-field-splitting value. Thus, there are a total of 30 possible allowed transitions (ΔM_s = 1) for each magnetic field orientation. A detailed study of the ESR spectra of a single crystal is now being carried out. The ESR spectrum of manganese doped with the $[Mg(terpy)(N_3)_2]_2\cdot 2H_2O$ homologous compound shows the hyperfine structure of a manganese ion with no detectable single-ion zero-field splitting. The calculated hyperfine parameter value, A = 92 G (85.9 × 10^{-4} cm^{-1}), is in good accord with values observed for Mn(II) compounds.[14]

The magnetic susceptibility of $[Mn(terpy)(N_3)_2]_2\cdot 2H_2O$ has been measured throughout the temperature range 4.2–200 K. The thermal variations of both the reciprocal molar susceptibility and $\chi_m T$ are shown in Figure 3. The variation of the reciprocal molar susceptibility data versus temperature is not well described by the Curie–Weiss law, even at higher temperatures, indicating the existence of considerable magnetic interactions in the compound. The $\chi_m T$ product increases with decreasing temperature from a value of 4.82 cm^3 K mol^{-1} at 200 K, reaching a maximum at a value of 7.50 cm^3 K mol^{-1}. The magnetic susceptibility data can be analyzed in terms of the dipolar coupling approach for a Mn(II) dimer. The expression for the magnetic susceptibility of the manganese(II) dimer, derived from Van Vleck's equation, is

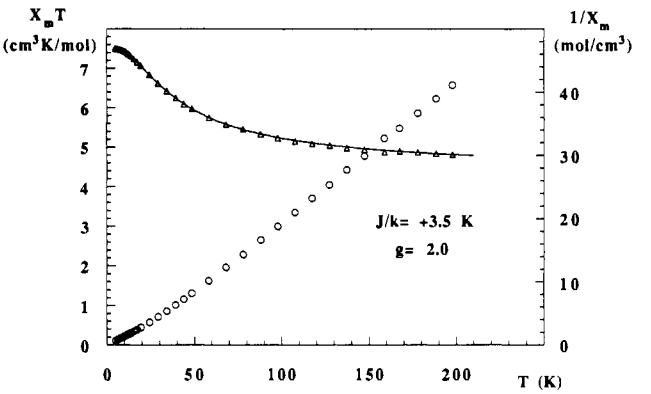

Figure 3. Thermal variation of the reciprocal susceptibility and $\chi_m T$ for the $[Mn(terpy)(N_3)_2]_2\cdot 2H_2O$ dimer.

$$\chi_A = (3N\beta^2g^2/3kT)\{[55 + 30\exp(10X) + 14\exp(18X) + 5\exp(24X) + \exp(28X)]/[11 + 9\exp(10X) + 7\exp(18X) + 5\exp(24X) + 3\exp(28X) + \exp(30X)]\}$$

$$X = -J/kT$$

In this particular case there should be virtually no mixing in of excited states by spin–orbit coupling. The fit following the above expression allows an evaluation of the intradimer exchange integral J for the compound. The calculated solid line in Figure 3 shows excellent agreement with the observed values (triangles), providing the following parameters: J/k = +3.5 K and g = 2.0.

The magnetic behavior indicates the existence of an intradimer ferromagnetic exchange interaction. The population of the molecular ground state S = 5 increases the value of $\chi_m T$ with decreasing temperature up to the observed maximum. No decrease from this maximum is observed by the absence of a detectable zero-field splitting.

As shown for Cu(II) and Ni(II) dimers with this type of azide bridging,[1,3,7,15] the ferromagnetic interactions depend on the value of the bridging M–N(azide)–M angle. For copper(II) dimers, a theoretical value for the bridging angle of 103° has been predicted for accidental orthogonality to occur.[1,15] Experimental data for the nickel dimers indicate the same correlation (with a bridging angle larger than 102°).[7] For these end-on-azido systems ferromagnetism is found for all the bridging angles, even for

(14) Bencini, A.; Gatteschi, D. *Mol. Phys.* **1985**, *54*, 969.

(15) Kahn, O.; Sikorav, S.; Gouteron, J.; Jeannin, S.; Jeannin, Y. *Inorg. Chem.* **1983**, *22*, 2877.

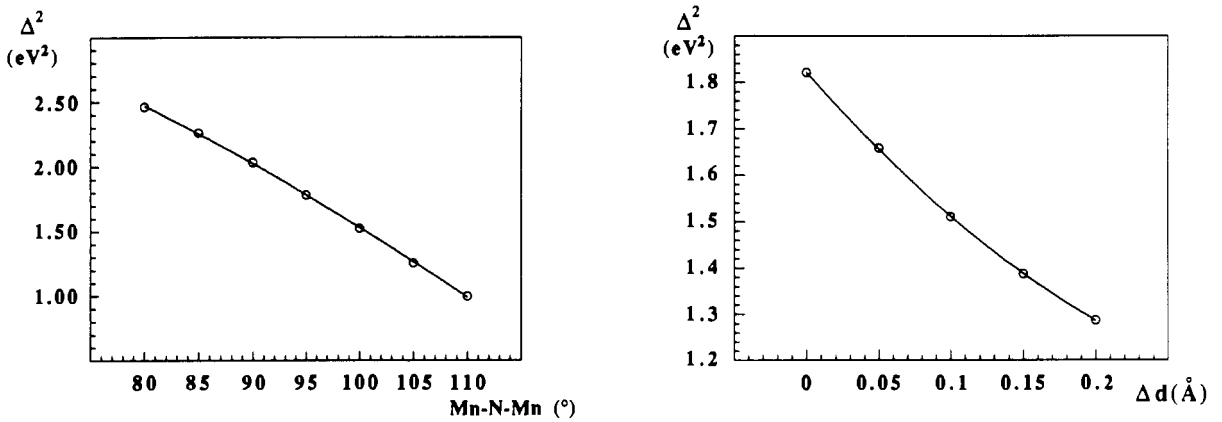

Figure 4. (a) Left: Variation of $\sum\Delta^2$ as a function of the bridging angle. (b) Right: Variation of $\sum\Delta^2$ as a function of the asymmetry (Δd) of the bridging unit.

those differing from accidental orthogonality with nonnegligible values for the gap between the magnetic orbitals.

Table 4 compiles various examples of edge-sharing Mn(II) bioctahedra.[16-25] Only oxygen and chlorine bridges have been found for these compounds. Due to the difference between the ligands of these compounds, structural comparisons must be carefully made. However, a larger asymmetry is observed for the azido bridging unit in comparison to the corresponding to the other bridging ligands. All the magnetically characterized compounds in Table 4 show antiferromagnetic interactions except the title compound. In spite of the different types of compounds, a drecrease in the antiferromagnetic interactions seems to be observed upon increasing the asymmetry (Δd) of the bridging unit.

The global value of the exchange parameter can be viewed as the sum of the antiferromagnetic contribution (J_{AF}), which depends on the splitting of the pairs of MO's, and the ferromagnetic contribution (J_F), which depends on the two-electron integrals. Only when J_{AF} is zero or negligible is J_F predominant and the behavior ferromagnetic. Although EHMO calculations are not valid to analyze the ferromagnetic component they, however, can be used to evaluate the antiferromagnetic contribution in these kinds of compounds. In this paper, EHMO calculations have been performed on a modeled hexacoordinate Mn(II) end-on-azido dimer (**1**) by means of the CACAO[26] program.

The magnetic orbitals influencing the superexchange in this case are the five d orbitals with one electron each. The antiferromagnetic contribution, a function of the square of the gap (Δ^2) between the pairs of MO's derived from the five magnetic orbitals per Mn(II) ion, must be proportional to the sum $\sum\Delta^2 = \Delta^2(d_{x^2-y^2}) + \Delta^2(d_{z^2}) + \Delta^2(d_{yz}) + \Delta^2(d_{xz}) + \Delta^2(d_{xy})$. The influence of both the bridging angle and the asymmetry of the metal–bridge bonds has been analyzed (Figure 4). From this analysis, a decrease of antiferromagnetic contribution can be observed as the bridging angle (Figure 4a) and the asymmetry of the bonds

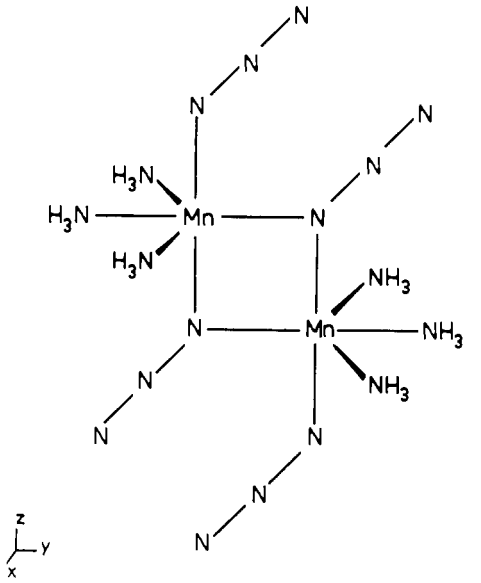

1

(Figure 4b) are increased. In spite of the title compound possessing a large bridging angle and the distortion favoring a decrease of AF interactions, the value of the gap between the highest and lowest orbitals is not negligible, and on the basis of this model, being mindful of its limitations, the interactions on these grounds would be expected to be antiferromagnetic. So, the ferromagnetic interactions in this complex must be better explained on the basis of the spin-polarization effect developed by Kahn and co-workers.[6] This model considers the in-plane π_g orbital (HOMO) of the azide anion, where the electron of the bridging nitrogen (α spin) is partially delocalized toward the two metal orbitals and consequently the electrons of the metals are likely to have β spins, favoring ferromagnetic interactions. On the basis of this model for the end-on-azido bridging, the coupling will be ferromagnetic for all values of distances and angles.

Acknowledgment. We are grateful for Grants-in-Aid for Scientific Research from both the Ministerio de Educación y Ciencia (DGICYT PB90-0549) and the Universidad del Pais Vasco/Euskal Herriko Unibertsitatea (UPV/EHU 130.310-EB017/92).

Supplementary Material Available: Tables giving anisotropic thermal parameters, hydrogen atom locations, crystal data and details of the structure determination, and distortion of the metal coordination polyhedron and a figure showing both the HOMO and LUMO magnetic orbitals and their variation with the bridging angle and the asymmetry of the bridging unit for the modelized dimer (5 pages). Ordering information is given on any current masthead page.

(16) Yu, S. B.; Wang, C. P.; Day, E. P.; Holm, R. H. *Inorg. Chem.* **1991**, *30*, 4067.
(17) Xianglin, J.; Zuohua, P.; Meicheng, S.; Youqi, T.; Depei, H.; Zihou, T.; Jinqi, Z. *Kexue Tongbao (Chin.)* **1983**, *28*, 1334.
(18) Willet, R. D. *Acta Crystallogr.* **1979**, *B35*, 178.
(19) Hodgson, D. J.; Schwartz, B. J.; Sorrell, T. N. *Inorg. Chem.* **1989**, *28*, 2226.
(20) Kessissoglou, D. P.; Butler, W. M.; Pecoraro, V. L. *Inorg. Chem.* **1987**, *26*, 495.
(21) Shoner, S. C.; Power, P. P. *Inorg. Chem.* **1992**, *31*, 1001.
(22) Downard, A. J.; McKee, V.; Tandon, S. S. *Inorg. Chim. Acta* **1990**, *173*, 181.
(23) Brooker, S.; McKee, V. *Inorg. Chim. Acta* **1990**, *173*, 69.
(24) Carducci, M. D.; Doedens, R. J. *Inorg. Chem.* **1989**, *28*, 2492.
(25) Caneschi, A.; Gatteschi, D.; Laugier, J.; Rey, P.; Zanchini, C. *Inorg. Chem.* **1989**, *28*, 1969.
(26) Mealli, C.; Proserpio, D. M. Computer Aided Composition of Atomic Orbitals (CACAO Program), PC version, July 1992, kindly supplied by C. Mealli. See also *J. Chem. Educ.* **1990**, *67*, 399.